SYSTEM IDENTIFICATION OF SOIL-STRUCTURE INTERACTION MECHANISMS FOR BUILDING STRUCTURES

D. S. Kusanovic, E. Esmaeilzadeh Seylabi, D. M. Asimaki

Department of Mechanical and Civil Engineering,
The California Institute of Technology, Pasadena, USA.

Abstract

We quantify the effects of dynamic soil-structure-interaction on building structures using system-identification techniques and finite element simulations. We develop analytic expressions for distributed spring and dashpot elements at the soil-foundation interface in terms of dimensionless variables. A system-identification approach based on Extended-Kalman-Filter is employed to estimate the *true* soil impedance as seen from the building-foundation system. The impedances estimated are next used to span the range of applicability of the proposed soil impedance model using nonlinear curve-fitting. We find good-agreement between the proposed flexible-based-model and the full finite element-model in period lengthening, radiation damping, time-history responses and their frequency contents.

Introduction

The accuracy of numerical models in civil engineering to predict the linear or nonlinear responses of structures depends among other phenomena on how well sources of energy dissipation and interaction processes are modeled. Energy dissipation mechanisms in the last decades has been considered through a series of simplified models: for instance, energy dissipation in buildings has been represented using mathematical models based on *viscous damping*. The basic idea is to combine all the sources of energy dissipation -- especially those which may be impractical, too complex, or not fully understood -- into a simple set of viscous parameters. Although it has been well established that some of the dissipation mechanisms do not behave in a viscous manner (Bernal 1994, Hall 2006), this inconsistency is frequently ignored in engineering practice because it simplifies the analysis (Jacobsen 1930) and produces reasonable results (Beck 1980). On the other hand, *soil-structure-interaction* (SSI) modeling is most of the time accounted in practice using *fixed-base* building models. In this approach modification of properties such as damping ratios is usually performed to account for mechanisms such as radiation damping. However, SSI effects can be considered in numerical analyses of building structures, more rigorously, using one of two methods: the *direct method* and the *substructure method*. In the *direct method*, the super-structure, the foundation, and the surrounding soil are explicitly taken into account, using for the most part the finite element method (Bathe 1996, and Hughes 2000); and since it is impossible to model the semi-infinite extent of the soil with finite number of the elements, appropriate boundary conditions have to be determined and applied to model the radiated energy (Lysmer 1969, and Basu 2003). Due to the computational time, memory constraints, and numerical modeling expertise involved in implementing the direct method, the state-of-the-practice has adopted the *substructure method*

(Wolf 1985, and NEHRP 2013). In this case, the problem is divided into two systems: *the superstructure* and the *soil-foundation* sub-systems. The soil-foundation system is first represented as force-deformation relationships in a representative frequency, known as *impedance functions*, which are then applied to the nodes along the soil-foundation interface to model the dynamic interaction between soil-foundation and superstructure. However, this approach presents two major difficulties: (i) the superposition method only works when the soil behaves elastically, and (ii) the representative frequency of the combined system at which the impedance functions respond is not clear. In order to address the issues presented in the *substructure method*, we propose an inference technique based on extended Kalman filtering (EKF) to estimate the values of the dynamic soil-spring and soil-dashpot elements to account for the dynamic response of the coupled building-foundation system. The identified soil-spring and soil-dashpot elements are employed to derive closed-form parametric expressions for the distributed soil-stiffness and soil-dashpot elements. Although the presented framework is here demonstrated to estimate the impedance functions of linear soil-structure problems, it is general enough that it can be extended to the case that both the structure and the surrounding soil are nonlinear.

The remainder of the paper is organized as follows: in §2 and §3, we use dimensional analysis to derive analytic expressions of the soil spring and dashpot coefficients as seen from the building foundation. We calibrate these expressions using a Bayesian identification approach based on Extended-Kalman-Filter (EKF) formulated to minimize the error between the *full-finite-element-model* (direct-method) and the *flexible-base-model* (substructure-method). In §4, we present analytical expressions for the period elongation and radiation damping of a flexible-base system on distributed horizontal and vertical springs, expressed as a function of an equivalent fixed-base system. We also present the equations of motion of a planar building that explicitly account for the building and foundation geometry as well as the soil-stiffness and energy radiated away from the building. Finally, in §5, we provide some discussion and concluding remarks regarding this new framework for modeling SSI problems using the *substructure method*.

The Problem Statement and Dimensional Analysis

The SSI continuum model we investigate in this study is composed of a building represented by its first-modal-height (h). The building, at the same time, is supported on a foundation system whose geometry is characterized by its half-foundation-length (B), and its foundation-depth (D). Moreover, the foundation system rests on a homogeneous soil half-space characterized by its shear-wave velocity (V_s). The response of the continuum model is approximated using the finite-element-method (Bathe 1996, and Hughes 2000). The material and elements are here considered to be isotropic linear and elastic, and no viscous damping is added so that the energy radiated away from the building comes only from radiation damping. Since, there are a large number of different SSI configurations that can be modeled, we employ *dimensional-analysis* to span the *dimensional-parameter space*, so that all possible cases or at least those in the range of applicability in civil engineering are covered. These parameters agrees with those proposed in Veletsos 1974, and they are listed below,

a) Structure-to-soil stiffness ratio:

$$\Pi_1 = \frac{h}{V_S\, T}$$

b) Building-aspect ratio:

$$\Pi_2 = \frac{h}{B}$$

c) Foundation-aspect ratio:

$$\Pi_3 = \frac{D}{B}$$

Three different buildings with fixed-base-fundamental period $T \approx (0.5, 1.0, 1.5)$ s, fixed-first-modal height $h \approx (15.0, 30.0, 40.0)$ m, foundation depth $D = (1.0, 2.5, 5.0)$ m, and supported on eleven distinct soils with shear wave velocities $V_s = (80, 100, 125, 150, 175, 200, 225, 250, 300, 400, 500)$ m/s are considered. These values will generate the *structure-to-soil stiffness ratio* to vary between $\Pi_1 \in [0.05 - 0.4]$, the *building-aspect ratio* to vary between $\Pi_2 \in [1.5 - 4.0]$, and the *foundation aspect ratio* to vary between $\Pi_3 \in [0.1 - 0.5]$. The range of parameters Π_1, Π_2 and Π_3, are chosen to be consistent with the range of applicability presented in Stewart 1999. The buildings employed in the dimensional analysis are schematically shown in Figure 1.

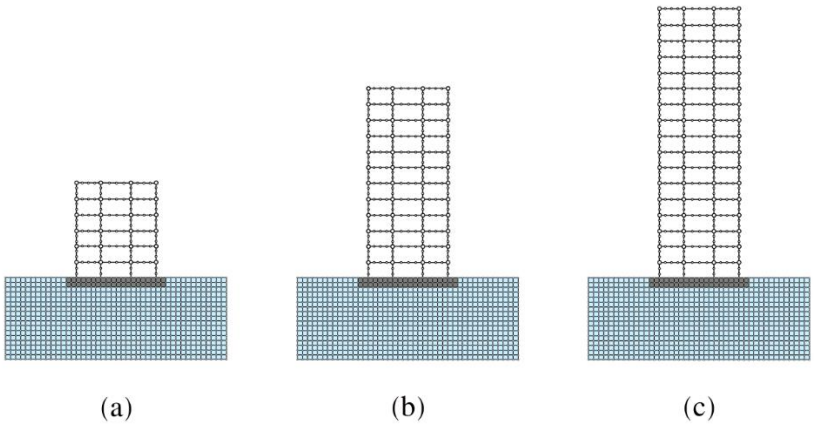

Figure 1. Building configurations employed in the dimensional analysis for the SSI problem.

Model Inversion for Soil-Structure Interaction Parameters

Once the *dimensional-parameter space* is defined, the *system-identification* can be applied to the SSI problems using the *substructure method*. The presented framework is thus performed in two stages: (i) as shown in Figure 2a, the *direct method* is employed from which a plane vertically-incident SV-wave is propagated upwards and the "true" building responses such as displacements or accelerations are recorded, then (ii) as shown in Figure 2b, the *substructure method* is employed in which the surrounding soil is replaced by a set of spring and dashpot

elements all over the foundation interface to emulate the soil inertia, stiffness and energy radiated away from the building. Such soil-spring and soil-dashpot elements are updated so that the error between the *direct-method* and the *substructure-method* is minimized. This approach ensures that information of the higher modes are implicitly considered in the estimation of the soil spring and dashpot elements. As part of this procedure, for the given set of spring and dashpot elements, we need to solve the semi-discrete Equation (1).

$$\mathbf{M}\,\ddot{\boldsymbol{u}}(\widehat{\boldsymbol{\theta}}) + \mathbf{C}(\widehat{\boldsymbol{\theta}})\,\dot{\boldsymbol{u}}(\widehat{\boldsymbol{\theta}}) + \mathbf{K}(\widehat{\boldsymbol{\theta}})\,\boldsymbol{u}(\widehat{\boldsymbol{\theta}}) = -\boldsymbol{L_g}\ddot{u}_{FFM}(t), \qquad (1)$$

where the variable $\ddot{u}_{FFM}(t)\ \epsilon\ \mathbb{R}$ represents the free-field ground motion signal at time t. The vector $\boldsymbol{L_g}\ \epsilon\ \mathbb{R}^n$ represents the earthquake influence vector that acts on the system, i.e., the vector that quantifies the inertial forces. The vectors $\boldsymbol{u}(\widehat{\boldsymbol{\theta}})\ \epsilon\ \mathbb{R}^n$, $\dot{\boldsymbol{u}}(\widehat{\boldsymbol{\theta}})\ \epsilon\ \mathbb{R}^n$ and $\ddot{\boldsymbol{u}}(\widehat{\boldsymbol{\theta}})\ \epsilon\ \mathbb{R}^n$ are the outputs of the system - here the displacement, velocity and acceleration respectively. $\mathbf{M}\ \epsilon\ \mathbb{R}^{n\times n}$, $\mathbf{C}(\widehat{\boldsymbol{\theta}})\ \epsilon\ \mathbb{R}^{n\times n}$ and $\mathbf{K}(\widehat{\boldsymbol{\theta}})\ \epsilon\ \mathbb{R}^{n\times n}$are the mass, damping, and stiffness matrices of the dynamical system, $\widehat{\boldsymbol{\theta}}\ \epsilon\ \mathbb{R}^{n_\theta}$ is the vector of system identifiable parameters, n the number of degree-of-freedom of the system, and n_θ the number of identifiable parameters.

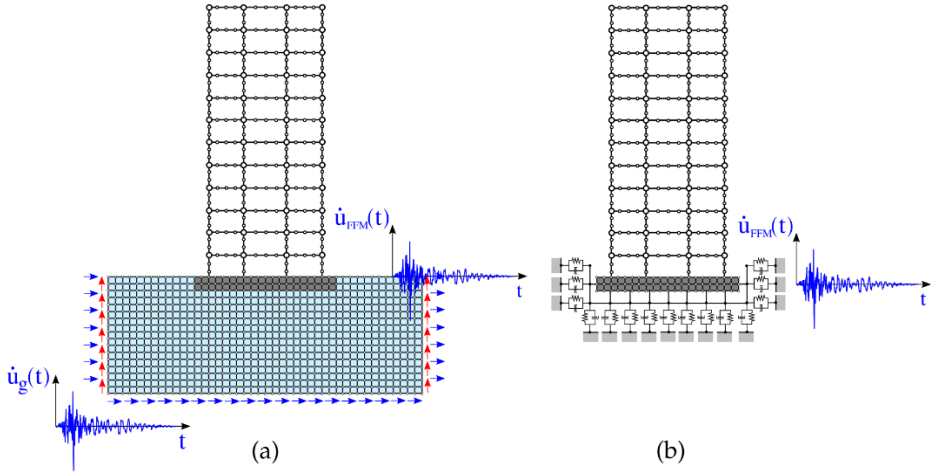

Figure 2. System-identification framework applied to SSI (a) Direct method from which the true responses are computed, and (b) Substructure method from which the spring and dashpot coefficients are estimated.

In the *direct-method*, the input-ground motion $\dot{u}_g(t)$ is prescribed as an effective force function at the base of the model at each soil node (Lysmer 1969, Asimaki 2004). For this purpose, a Ricker-wavelet (Ricker 1945) is selected and given in Equation (2),

$$\dot{u}_g(t) = (1 - 2\gamma(t - t_0)^2)e^{-\gamma(t-t_0)^2}, \qquad (2)$$

where $\gamma = (\pi f_0)^2$, $f_0 = 2$ [Hz] is the characteristic frequency, t_0 is the time position where the velocity will become maximum. On the other hand, the absorbing boundary conditions are implemented according to (Lysmer 1969, Asimaki 2004). Once the responses of the *direct-method* are obtained, an estimation method based on *Extended-Kalman-Filter* (EKF) is applied

to identify the soil-spring and soil-dashpot elements. The estimation process assumes that soil-spring and soil-dashpot coefficients are time-invariant, and therefore their evolution is modeled as a random walk process using a time invariant zero mean Gaussian noise with a known covariance matrix as it is given in Equation (5). We also assume that the error due to the misfit between the measured and predicted responses can be represented as a time invariant zero mean Gaussian noise with a known covariance matrix as it is given in Equation (6). Then, the parameter and measurement equations are given as follows:

$$\boldsymbol{\theta}_k = \boldsymbol{\theta}_{k-1} + \boldsymbol{q}_{k-1}, \quad (3)$$

$$\boldsymbol{y}_k = h_k(\boldsymbol{\theta}_k) + \boldsymbol{r}_k, \quad (4)$$

$$\boldsymbol{q}_k \sim (\boldsymbol{0}, \boldsymbol{Q}_k), \quad (5)$$

$$\boldsymbol{r}_k \sim (\boldsymbol{0}, \boldsymbol{R}_k), \quad (6)$$

where $\boldsymbol{\theta}_k \in \mathbb{R}^{n_\theta}$ is the parameter vector at the $k-$th updated stage. The variable $\boldsymbol{y}_k \in \mathbb{R}^{n_y}$ is the response vector of the system. $h_k(\boldsymbol{\theta}_k)$ is the non-linear vector-value measurement function such that, h: $\mathbb{R}^{n_\theta} \rightarrow \mathbb{R}^{n_y}$. $\boldsymbol{q}_k \in \mathbb{R}^{n_\theta}$ and $\boldsymbol{r}_k \in \mathbb{R}^{n_y}$ are the process and observation noises which are both assumed to be zero mean multivariate Gaussian noises with covariance $\boldsymbol{Q}_k \in \mathbb{R}^{n_\theta \times n_\theta}$ and $\boldsymbol{R}_k \in \mathbb{R}^{n_y \times n_y}$ respectively.

The EKF algorithm is then employed in the *substructure-method* to update the values of the soil-spring and soil-dashpot elements. A total of 99 identifications are required to modestly span the *dimensional-parameter space*. Then, a non-linear curve-fitting is performed to this set of coefficients to find a relation. In the dimensional analysis we have not considered ν as the influencing parameter, however the normalizing factor is written in terms of the Poisson's ratio such that the structure of each non-linear impedance function resembles the well-known static stiffness of homogeneous soil in half-space in the three dimensional setting. In particular, these equations take the following form

$$k_x(\hat{\boldsymbol{\pi}}, \hat{\boldsymbol{\alpha}}, \hat{\boldsymbol{\beta}}) = \frac{\rho_s {V_s}^2}{1-\nu} B \; \frac{\beta_0}{\beta_1 + \left(\frac{B}{B_r}\right)^{\beta_2}} \left[\alpha_0 + \alpha_1 \left(\frac{h}{B}\right)^{\alpha_2} \left(\frac{D}{B}\right)^{\alpha_3} \left(\frac{h}{V_S T}\right)^{\alpha_4}\right] \quad (7)$$

$$k_z(\hat{\boldsymbol{\pi}}, \hat{\boldsymbol{\alpha}}, \hat{\boldsymbol{\beta}}) = \frac{\rho_s {V_s}^2}{1-\nu} D \; \frac{\beta_0}{\beta_1 + \left(\frac{B}{B_r}\right)^{\beta_2}} \left[\alpha_0 + \alpha_1 exp\left(\alpha_2 \frac{h}{B}\right) exp\left(\alpha_2 \frac{D}{B}\right) \left(\frac{h}{V_S T}\right)^{\alpha_4}\right] \quad (8)$$

$$c_x(\hat{\boldsymbol{\pi}}, \hat{\boldsymbol{\alpha}}, \hat{\boldsymbol{\beta}}) = \frac{\rho_s {V_s}^2}{1-\nu} TD \; \frac{\beta_0}{\beta_1 + \left(\frac{B}{B_r}\right)^{\beta_2}} \left[\alpha_0 + \alpha_1 \left(\frac{h}{B}\right)^{\alpha_2} \left(\frac{D}{B}\right)^{\alpha_3} \left(\frac{h}{V_S T}\right)^{\alpha_4}\right] \quad (9)$$

$$c_z(\hat{\boldsymbol{\pi}}, \hat{\boldsymbol{\alpha}}, \hat{\boldsymbol{\beta}}) = \frac{\rho_s {V_s}^2}{1-\nu} TD \; \frac{\beta_0}{\beta_1 + \left(\frac{B}{B_r}\right)^{\beta_2}} \left[\alpha_0 + \alpha_1 \left(\frac{h}{B}\right)^{\alpha_2} \left(\frac{D}{B}\right)^{\alpha_3} \left(\frac{h}{V_S T}\right)^{\alpha_4}\right] \quad (10)$$

where $\widehat{\boldsymbol{\pi}} \epsilon \mathbb{R}^{n_p}$ is the *vector of dimensional parameters*, $\widehat{\boldsymbol{\alpha}} \epsilon \mathbb{R}^5$ is the vector of non-linear coefficient to be determined employing the data provided with the 99 analyses, and $\widehat{\boldsymbol{\beta}} \epsilon \mathbb{R}^3$ is the *influence-foundation vector*. Table I provides the estimated values that minimize the discrepancies between the data of the 99 configurations. The foundation influence coefficient vector is given as $\widehat{\boldsymbol{\beta}} = (1.16142, 0.05551, 1.93470)$, and the reference foundation length is taken as $B_r = 10\ [m]$ in the presented analysis.

Soil	Non-linear Regression Coefficients				
Impedance	α_0	α_1	α_2	α_3	α_4
k_x	0.007	0.2533	-1.6191	-0.8519	2.1399
k_z	0.0237	0.1785	0.178	-9.0619	-0.0938
c_x	0.0009	0.0205	-1.1906	-2.1511	3.1718
c_z	0.0002	0.0074	-1.0508	-1.1192	0.9116

Table I. Coefficients for the normalized soil-structure-interaction function for the soil coefficients provided in equations (7), (8), (9), and (10) respectively.

Validation of Soil-Spring and Soil-Dashpot Elements

A new set of fifteen more buildings with different topology are generated. The first-modal building parameter as well as the soil impedances for the new candidates are summarized in Table II. Figure 3 represents the configurations represented in Table II in the *dimensional-parameter space* Ω_{DS}. The blue-rectangle represents the *dimensional-analysis space* Ω_{DA} for which the inversion was carried out, and the size of these dots represents the intensity or susceptibility of the building frame to the SSI effect.

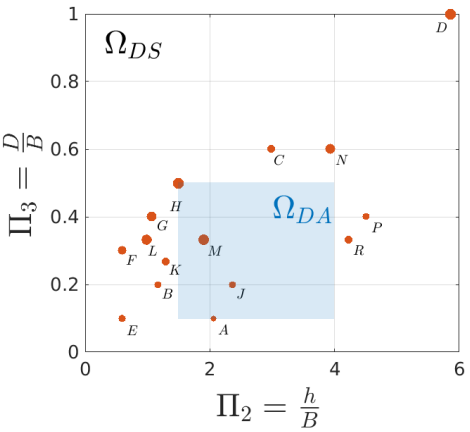

Figure 3. The validation cases represented in the dimension analysis domain.

In figures 4 - 6 the time history responses at the first-modal height for the total-horizontal displacement $\widehat{\Delta}_X^h$ and the total-vertical displacement $\widehat{\Delta}_Y^h$ are represented in solid-blue line and solid-red line for both the *direct-method* and the *substructure-method* respectively. In addition, the total-horizontal displacement of the roof $\widehat{\Delta}_X^r$ and the total-horizontal displacement of the ground level $\widehat{\Delta}_X^g$ are displayed in a similar fashion. Moreover, the frequency contents of such

signals for the total displacement are represented in the same figures, along with the normalized representation of the evaluated frame so that the different topologies considered in these three cases become much clearer. It can be seen in these figures that a good-agreement is achieved in both the total displacements at different levels, and the frequency content of the corresponding signals.

Frame Name	Fixed Period	Found. Mass	Building Dimensions			Shear Velocity	Dimensional Parameters		
			B	D	h				
	s	10^5 kg	m	m	m	V_s m/s	Π_1	Π_2	Π_3
A	0.25	0.125	5.0	0.5	10.270	250	0.162	2.05	0.10
B	0.35	0.250	5.0	1.0	5.820	80	0.208	1.16	0.20
C	0.40	0.500	5.0	3.0	14.940	150	0.248	2.99	0.60
D	0.90	0.500	5.0	5.0	29.320	120	0.272	5.86	1.00
E	0.25	0.500	10.0	1.0	5.890	130	0.181	0.59	0.10
F	0.28	0.500	10.0	3.0	5.900	100	0.214	0.59	0.30
G	0.60	0.500	10.0	4.0	10.670	75	0.237	1.07	0.40
H	0.48	0.500	10.0	5.0	14.980	115	0.274	1.50	0.50
J	1.08	0.500	15.0	3.0	35.380	190	0.172	2.36	0.20
K	0.65	0.500	15.0	4.0	19.350	150	0.198	1.29	0.27
L	0.49	0.500	15.0	5.0	14.830	120	0.253	0.99	0.33
M	0.85	0.500	15.0	5.0	28.510	125	0.268	1.90	0.33
N	0.53	0.500	5.0	3.0	19.650	150	0.247	3.93	0.60
P	1.75	0.500	10.0	4.0	45.100	150	0.172	4.51	0.40
R	2.13	0.500	15.0	5.0	63.440	150	0.198	4.23	0.33

Table II. Building parameters employed in the validation process.

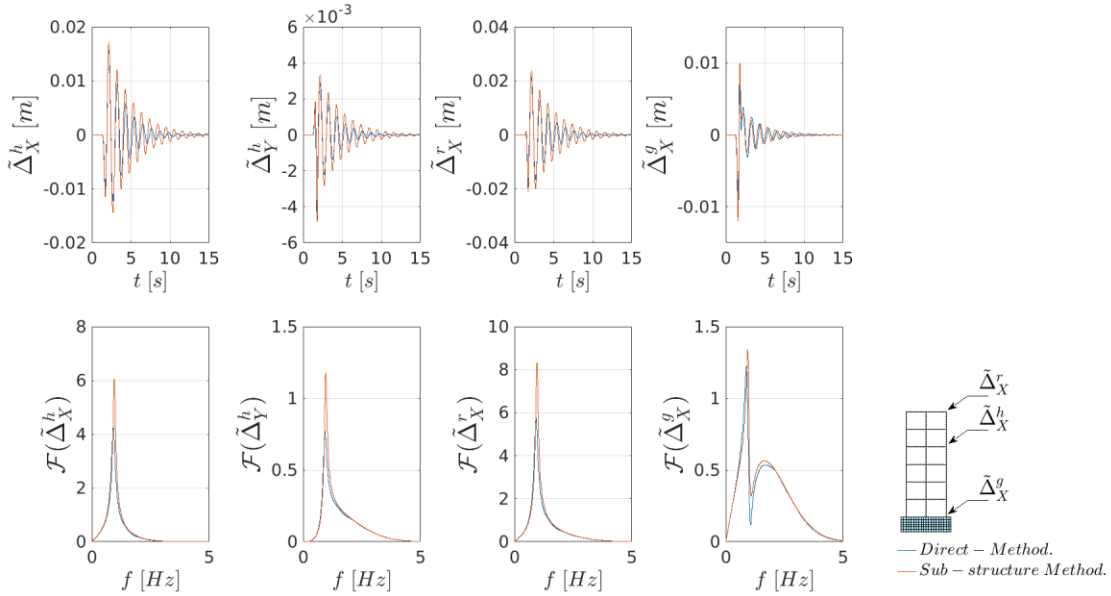

Figure 4. (Frame C): The parameters considered in the analysis are for the building a fixed-fundamental period T = 0.40 s, and a fixed-first modal height h = 14.94 m. The foundation dimensions are a half-length B = 5 m, and a foundation depth D = 3.0 m. The soil shear velocity is Vs = 150 m/s.

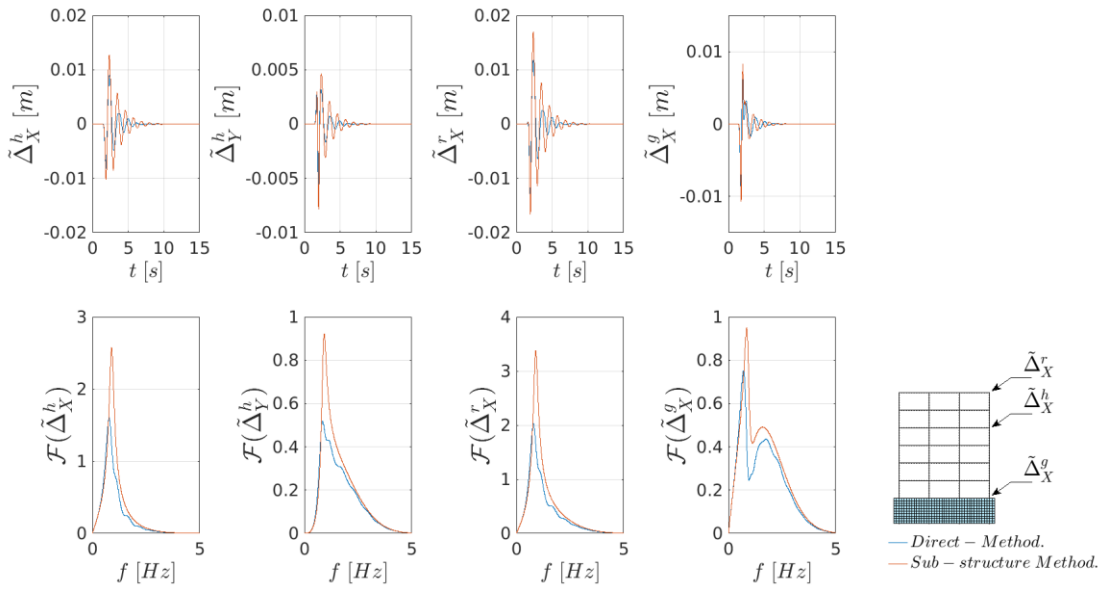

Figure 5. (Frame H): The parameters considered in the analysis are for the building a fixed-fundamental period T = 0.48 s, and a fixed-first modal height h = 14.98 m. The foundation dimensions are a half-length B = 10 m, and a foundation depth D = 5.0 m. The soil shear velocity is Vs = 115 m/s.

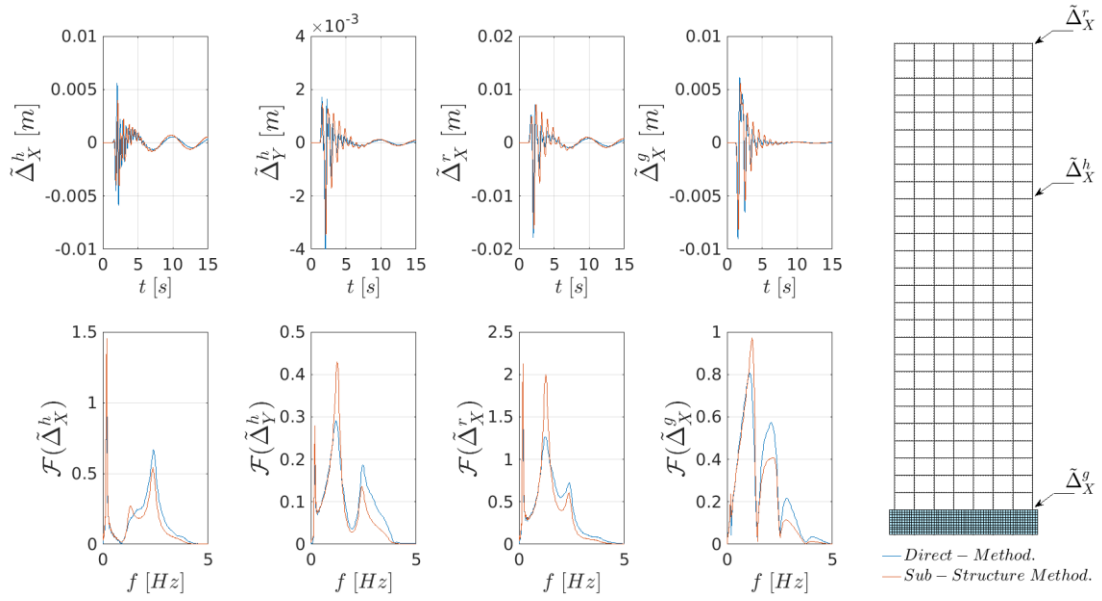

Figure 6. (Frame R): The parameters considered in the analysis are for the building a fixed-fundamental period T = 2.13 s, and a fixed-first modal height h = 63.44 m. The foundation dimensions are a half-length B = 15 m, and a foundation depth D = 5.0 m. The soil shear velocity is Vs = 150 m/s.

Table III quantifies the discrepancies between the *direct-method* and the *substructure-method*. In particular, the error associated to maximum displacement in the complete model is evaluated. The period elongation as well as the radiation damping error are also computed.

Finally the slope as well as the correlation of the time-series between the *full-finite-element model* and the *substructure-finite-element model* are computed at each node, and the maximum discrepancy between them is reported in Table III. The slope of such correlation measures how-well the simulated signal scales from the true response, and the Pearson's coefficient measures how-similar the signals are. It can be noted in Table III that the response signals of building frames M and J are very identical to the ones obtained using the *full-finite-element model*, when absolute quantities such as maximum displacement responses, period elongation, and global damping of the signal are compared. These results are consistent since these frames are inside the dimensional-design space, and we expect a good-agreement in this area. On the contrary, one should give special consideration to frame D, in which the signals, even though capture the maximum amplitude and the period elongation, fail in capturing the signal's pattern. This validation point is placed on purpose far from the *design space*, and therefore it was expected not to have a good-agreement since the extrapolation process becomes inaccurate. However, as it was pointed out earlier for all those frames that are near the dimensional-design space the results in displacements and frequency contents are quite accurate. Another important point to highlight is that for those buildings which are flexible, i.e., frame J, M, P and R, the higher mode responses are well-captured employing the *substructure-method* and the soil-spring and soil-dashpot elements presented here.

Model Reduction for Soil-Structure Interaction Parameters

We next present analytic expressions for the *period elongation* and *radiation damping* of an equivalent fixed-base system, as a function of the soil-stiffness (k_x, k_z) and soil-dashpot (c_x, c_z) elements which are distributed along the soil-foundation interface. In this analysis, we assume that the distributed soil-stiffness and soil-dashpot coefficients are known, moreover, the expressions derived hereafter can be considered as an extension of the ones proposed in Givens 2016, Stewart 1999 since we generate the coupling restoring moment term in a consistent manner by using both horizontal and vertical spring elements, as it is shown in Figure 7.

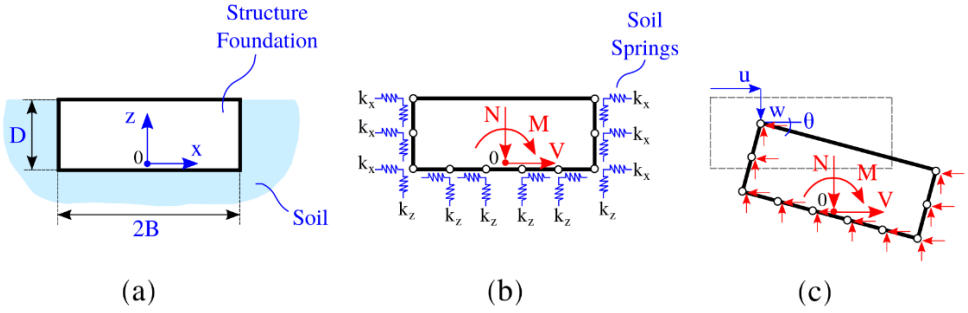

Figure 7. The soil-foundation system. (a) Geometry of the foundation system, (b) Modeling of the soil continuum as distributed springs, and (c) Free-body diagram of the foundation.

In Figure 7a, the external forces applied to the system are an axial force N, a shear force V, and a moment M. These forces are such that $N, V, M: f\left(\boldsymbol{u}(x,z)\right) \rightarrow \mathbb{R}$, where $\boldsymbol{u}(x,z)$ represents the displacement field. The restoring forces exerted by the soil are represented as springs acting over the foundation perimeter as shown in Figure 7b. Moreover, the foundation is assumed to be rigid so that the displacement field can be described with three degrees-of-

freedom as shown in Figure 7c. Next, and without loss of generality, we assume that the distributed horizontal springs k_x and vertical springs k_z are constant over the soil-foundation interface, this is basically to assume that $k_x(x,z) = k_x$, and $k_z(x,z) = k_z$. It should be noted that we used the same assumption for model inversion, as elaborated before. Satisfying equilibrium of forces and moment for the system presented in Figure 7c results in the lumped stiffness and damping matrices written in the following compact form.

$$\boldsymbol{\Lambda} = \begin{bmatrix} \Lambda_{zz} & 0 & 0 \\ 0 & \Lambda_{xx} & \Lambda_{x\theta} \\ 0 & \Lambda_{x\theta} & \Lambda_{\theta\theta} \end{bmatrix} = \begin{bmatrix} 2\,\lambda_z(D+B) & 0 & 0 \\ 0 & 2\,\lambda_x(D+B) & \lambda_x D^2 \\ 0 & \lambda_x D^2 & \frac{2}{3}\lambda_x D^3 + \frac{2}{3}\lambda_z B^3 + 2\,\lambda_z B^2 D \end{bmatrix}, \quad (11)$$

where the matrix $\boldsymbol{\Lambda}$ represents either the stiffness or damping matrix of the foundation system, and λ the distributed spring or dashpot coefficient. A dynamic analysis can now be performed to the simplified flexible-base system as the one shown in Figure 8b, in which the surrounding soil is replaced by uniform distributed horizontal and vertical springs k_x, k_z and dashpots c_x, c_z. Equation (11) allows us to compute the reduced reactive soil forces that must be added to the foundation so that the dynamic equilibrium using Dalambert's principle can be carried out.

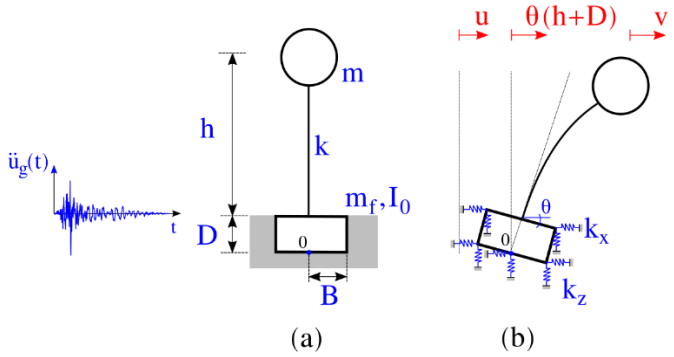

Figure 8. Reduced soil-structure-interaction model for dynamic analysis.

In this regard, the equation of motion is written as

$$\begin{bmatrix} m & m & m(h+D) \\ m & m+m_f & m(h+D)+m_f\frac{D}{2} \\ m(h+D) & m(h+D)+m_f\frac{D}{2} & m(h+D)^2+m_f\frac{D^2}{4}+I_0 \end{bmatrix} \begin{bmatrix} \ddot{u} \\ \ddot{v} \\ \ddot{\theta} \end{bmatrix} + \begin{bmatrix} c & 0 & 0 \\ 0 & c_{xx} & c_{x\theta} \\ 0 & c_{x\theta} & c_{\theta\theta} \end{bmatrix} \begin{bmatrix} \dot{u} \\ \dot{v} \\ \dot{\theta} \end{bmatrix}$$
$$+ \begin{bmatrix} k & 0 & 0 \\ 0 & k_{xx} & k_{x\theta} \\ 0 & k_{x\theta} & k_{\theta\theta} \end{bmatrix} \begin{bmatrix} u \\ v \\ \theta \end{bmatrix} = - \begin{bmatrix} m \\ m+m_f \\ m(h+D)+m_f\frac{D}{2} \end{bmatrix} \ddot{u}_g(t), \quad (12)$$

where the variables u, v, and θ are the relative displacement of the foundation, the relative displacement of the mass and the total rotation of the foundation respectively. The variables $\dot{u}, \dot{v}$, and $\dot{\theta}$ are the velocities, and $\ddot{u}, \ddot{v}$ and $\ddot{\theta}$ are the accelerations in the above mentioned degrees of

freedom. The variables k and c represent, respectively, the fixed-base stiffness and viscous damping of the building, and $k_{xx}, k_{x\theta}, k_{\theta\theta}, c_{xx}, c_{x\theta}$ and $c_{\theta\theta}$ are the soil-stiffness and soil-dashpot matrix coefficients provided in Equation (11). The variable m is the mass of the fixed-base building, m_f the mass of the foundation, and I_0 the rotational inertia of the foundation, and lastly $\ddot{u}_g(t)$ is the ground acceleration.

The stiffness and damping matrices in Equation (11) can also be employed to replace the simplified flexible-base system of modified height $\bar{h} = h + D$, stiffness $k \in \mathbb{R}^+$, structural damping $\beta \in \mathbb{R}^+$, supported by a distributed horizontal spring $k_x \in \mathbb{R}^+$and distributed vertical springs $k_z \in \mathbb{R}^+$with an equivalent fixed-base single-degree-of-freedom system with mass $m \in \mathbb{R}^+$, modified-stiffness $\tilde{k} \in \mathbb{R}^+$, modified-fundamental period $\tilde{T} \in \mathbb{R}^+$, and modified damping $\beta_0 \in \mathbb{R}^+$as it is presented in Givens 2016, Stewart 1999. This idea is depicted in Figure 9.

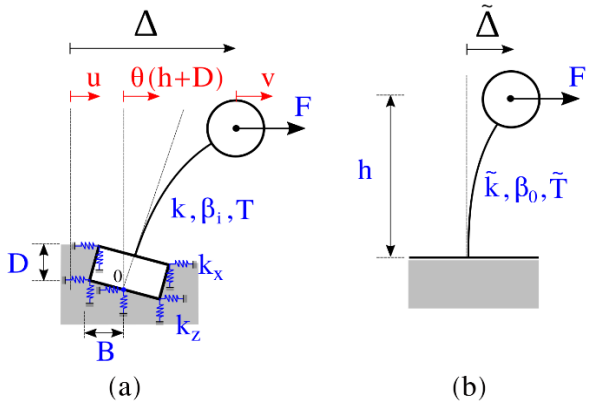

Figure 9. Model reduction from (a) the simplified flexible-base system into (b) the equivalent fixed-base system.

It can be shown that the *period elongation* is defined as follows:

$$\frac{\tilde{T}}{T} = \sqrt{1 + \frac{k}{k_{xx}\, k_{\theta\theta} - k_{x\theta}{}^2}\left(\bar{h}^2 k_{xx} - 2\,\bar{h}\, k_{x\theta} + k_{\theta\theta}\right)}, \qquad (13)$$

Note that in Equation (13) when the stiffness $k_{x\theta} = 0$, the expression reduces to the same as the one presented in Givens 2016, Stewart 1999. Following a similar procedure as presented in Givens 2016, Stewart 1999 we obtain the reduced *foundation-damping* provided in Equation (14),

$$\beta_0 = \frac{\beta_i}{\left(\frac{\tilde{T}}{\overline{T}}\right)^2} + \frac{\beta_x}{\left(\frac{\tilde{T}}{T_x}\right)^2}\left(\frac{1-\bar{h}\frac{k_{x\theta}}{k_{\theta\theta}}}{1-\frac{{k_{x\theta}}^2}{k_{xx}\,k_{\theta\theta}}}\right)^2 - \frac{2}{\left(\frac{\tilde{T}}{T_x}\right)}\frac{\beta_{x\theta}}{\left(\frac{\tilde{T}}{T_\theta}\right)}\frac{k_{x\theta}}{\sqrt{k_{xx}\,k_{\theta\theta}}}\frac{\left(1-\frac{k_{x\theta}}{\bar{h}\,k_{xx}}\right)\left(\bar{h}\frac{k_{x\theta}}{k_{\theta\theta}}-1\right)}{\left(1-\frac{{k_{x\theta}}^2}{k_{xx}\,k_{\theta\theta}}\right)^2}$$
$$+ \frac{\beta_\theta}{\left(\frac{\tilde{T}}{T_\theta}\right)^2}\left(\frac{1-\frac{k_{x\theta}}{\bar{h}\,k_{xx}}}{1-\frac{{k_{x\theta}}^2}{k_{xx}\,k_{\theta\theta}}}\right)^2, \qquad (14)$$

where we define the *translational period* as $T_x = 2\pi\sqrt{\frac{m}{k_{xx}}}$ and the *rocking period* as $T_\theta = 2\pi\sqrt{\frac{m\bar{h}^2}{k_{\theta\theta}}}$. Note once again that when the stiffness $k_{x\theta} = 0$ in Equation (14) the expression reduces to the one presented in Givens 2016, Stewart 1999 for the foundation damping.

Global Soil-Structure-Interaction effects on Buildings

In this section, equations (13) and (14) are employed to estimate the *period lengthening* and *radiation damping*. In addition, and in order to compare how much these values deviate, the so-called and well-accepted modified-Bielak-method - described in details in Jacobo 1975, Stewart 1999 - is employed. However, the modified-Bielak-method requires the impedance function of the soil to be prescribed. In order to deal with this situation, the procedure described in Seylabi 2016 is employed to compute the translational and rotational impedance functions of the half-space soil in plane strain condition assuming a rigid foundation.

Figures (10) shows the period elongation and radiation damping computed using the modified-Bielak-method and the system-identification method based on the Kalman filtering for different foundation aspect ratios. As shown, a good-agreement between the proposed expressions and the one obtained using modified-Bielak-method is achieved. On the one hand, it is evident that Equation (13) provides with more flexible models, but on the other hand, Equation (14) provides with less-dissipative values when they are compared with the modified-Bielak-method. A very close fit is however obtained for the three-buildings when the *foundation aspect ratio* is small (i.e., $\Pi_3 = 0.1$). The discrepancies must be attributed mainly to the fact that the estimated frequency of the interaction using the system-identification framework can be different from the one obtained using the modified-Bielak-method. Moreover, in the system-identification framework, we are implicitly compensating for kinematic interaction in the embedded cases as well as we are implicitly considering the spring and dashpot coupling terms. It can be seen in both equation (13) and (14) that mentioned coupling in the stiffness and damping matrices generate a slight increase in the period elongation ratio as well as a slight decrease in the radiation damping. It is indeed evident that if the term $k_{x\theta}$ is set to be zero, then the expression given in Equations (13) and (14) and the ones provided in Jacobo 1975, Stewart 1999 are totally equivalent. However, this small deviation plays an important role in the period elongation and radiation damping of the *reduced-model* when the foundation embedment becomes larger.

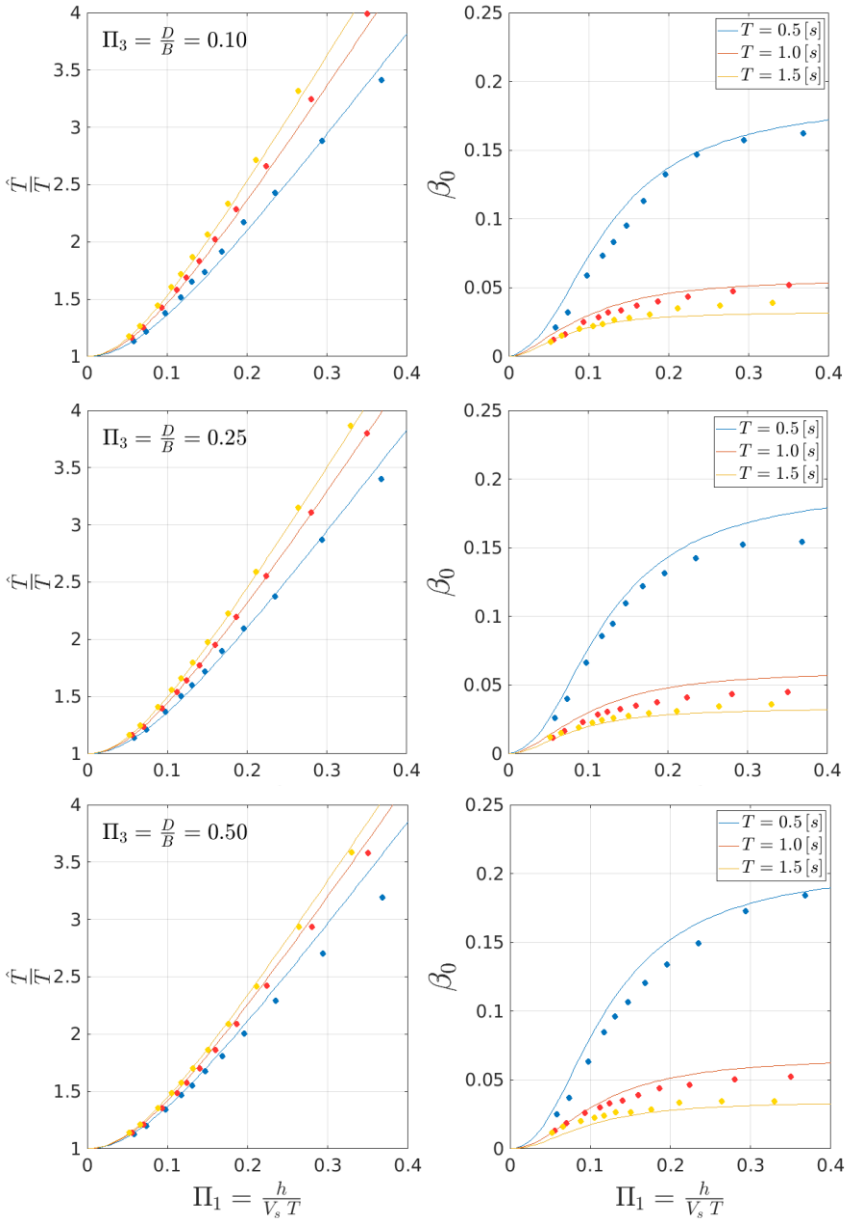

Figure 10. Period elongation ratio $\tilde{T}/T$ and radiation damping β_0 for the three buildings with $T = (0.507, 1.025, 1.531)$ s, supported on eleven homogeneous soil half-space with $V_s = (80, 100, 125, 150, 175, 200, 225, 250, 300, 400, 500)$ m/s. The solid-lines represent the modified-Bielak-method while the solid-dots represents equation (13) or (14) using the system-identification-method.

Summary and Conclusions

In this study, we first presented analytic expressions to estimate soil's impedance functions to account for inertial interaction and kinematic interaction in terms of dimensional parameters. In particular, the *structure-to-soil-stiffness ratio*, *foundation-aspect ratio*, and *building-aspect ratio* are chosen as dimensionless parameters in this framework. The distributed soil-spring and soil-dashpot elements identified using the Extended-Kalman-Filter are the one

that best represents the system interaction between the soil and the structure since it minimizes the error between the *direct-method* and the *substructure-method*. These soil-spring and soil-dashpot functions were then tested using the substructure-flexible-based-model to validate its accuracy and predictive power in several configuration systems. It is worth mentioning that the impedance expressions obtained using the EKF are assumed to be frequency independent. This assumption is not inaccurate since the frequency contents of earthquake signals in general varies between $0.2 - 10$ Hz, range in which the impedances of the homogeneous soil half-space are more-or-less constant. Another important aspect we consider is because of the building' symmetry the responses are dominated by their first-mode of vibration. However, higher-mode responses are well-captured employing the framework presented here. We second presented analytic expressions to evaluate the effects of period lengthening and radiation damping for a reduced-fixed-base system. The provided expressions can be considered as an extension to Givens 2016, Stewart 1999 since it incorporates the coupling term in the stiffness matrix as well as the damping matrix. In overall a good-agreement is reached not only for global parameters such as maximum displacements, period lengthening and radiation damping, but also for local responses such as time-history displacements at each node evaluated in terms of correlation between both the *direct-method* and the *substructure-method*.

Nevertheless, extrapolation far from the *dimensional-analysis design domain* represented in a blue rectangle in Figure 3 can produce large errors in global responses such as period elongation, and radiation damping. However, for almost all cases represented in this work, we note a good-agreement in both time history responses and their frequency content for the extrapolated values. The discrepancies are mostly attributed to the facts that (i) the extrapolation of the soil spring and dashpot elements using equations (7), (8), (9), and (10) is not exact, and (ii) the number of building frames considered in this analysis to span the whole dimensional-parameter space may not be enough—therefore a more refined sampling for *building-aspect ratio* (Π_2) and *foundation-aspect ratio* (Π_3) should be employed to provide with a much better approximation. Overall, extrapolation close to the *design domain* provides a very small error in terms of time history responses, maximum displacements, period lengthening and radiation damping when they are compared to the full-finite element model as it is presented in Table III.

Frame Name	Maximum Displacement Error	Period Elongation Error	Radiation Damping Error	Correlation Slope m	Correlation Pearson's R^2
A	0.0268	0.006	0.1017	1.0610	0.9660
B	0.1709	0.032	0.1073	1.1390	0.9677
C	0.1176	0.045	0.1073	1.1113	0.9212
D	0.2158	0.2131	0.3845	0.2394	0.2321
E	0.22	0.0874	0.1554	0.9772	0.8973
F	0.2407	0.0688	0.0096	1.1743	0.9462
G	0.2061	0.1204	0.1141	1.2246	0.8947
H	0.233	0.113	0.0893	1.2071	0.8689
J	0.1787	0.0491	0.0276	1.1088	0.8604
K	0.1787	0.0977	0.0663	1.1088	0.8604
L	0.1815	0.0794	0.0238	1.1250	0.9137
M	0.2341	0.0568	0.0164	1.1005	0.8913
N	0.013	0.0304	0.0124	0.9472	0.9252
P	0.171	0.004	0.1077	0.9070	0.7821
R	0.0895	0.0848	0.1321	0.7400	0.6713
max	0.013	0.004	0.0096	0.7400	0.6713
min	0.2407	0.1204	0.1554	1.2246	0.9677
Average	0.1615	0.0625	0.0765	1.0666	0.8833

Table III. Errors associated to response parameters employed in the validation process.

Acknowledgments

This study was supported partially by the California Geological Survey through Contract # 106-987. This support is gratefully acknowledged. Any opinions, findings, conclusions or recommendations expressed in this study are those of the authors and do not necessarily reflect the views of the sponsoring agency.

References

Bernal D., 1994. Viscous damping in inelastic structural response. Journal of Structural Engineering; 120(4):1240–1254.

Hall J., 2006. Problems encountered from the use (or misuse) of Rayleigh damping. Earthquake Engineering & Structural Dynamics.

Jacobsen L., 1930. Steady force vibration as influenced by damping, vol. 52. American Society of Mechanical Engineers.

Beck J, Jennings P., 1980. Structural identification using linear models and earthquake records, vol. 8. Earthquake Engineering Structural Dynamics.

Bathe K., 1996. Finite Element Procedures. Prentice-Hall International Series in, Prentice Hall.

Hughes T., 2000. The Finite Element Method: Linear Static and Dynamic Finite Element Analysis. Dover Civil and Mechanical Engineering, Dover Publications.

Lysmer J, Kuhlemeyer R., 1969. Finite Dynamic Model for Infinite Media. Reprint (University of California), Department of Civil Engineering, University of California, Institute of Transportation and Traffic Engineering, Soil Mechanics Laboratory.

Basu U, Chopra AK., 2003. Perfectly matched layers for time-harmonic elasto-dynamics of unbounded domains: theory and finite-element implementation. Computer Methods in Applied Mechanics and Engineering; 192(11):1337–1375.

Wolf JP., 1985. Dynamic soil-structure interaction. Upper Saddle, N.J.: Prentice-Hall. Security U, Agency FEM. Improvement of Nonlinear Static Seismic Analysis Procedures: Fema 440. Createspace Independent Publication.

Veletsos A, Meek J., 1974. Dynamic behavior of building-foundation systems. Earthquake Engineering & Structural Dynamics; 3(2):121–138.

Stewart JP, Seed RB, Fenves GL., 1999. Seismic soil-structure interaction in buildings. ii: Empirical findings. Journal of Geotechnical and Geo-environmental Engineering; 125(1):38–48.

Ricker N., 1945. The computation of output disturbances from amplifiers for true wavelet inputs. GEOPHYSICS; 10(2):207–220.

Assimaki D., 2004. Topography effects in the 1999 Athens earthquake: engineering issues in seismology. PhD Thesis, Massachusetts Institute of Technology. Dept. of Civil and Environmental Engineering.

Givens MJ, Mylonakis G, Stewart JP., 2016. Modular analytical solutions for foundation damping in soil-structure interaction applications. Earthquake Spectra; 32(3):1749–1768.

Stewart JP, Fenves GL, Seed RB., 1999. Seismic soil-structure interaction in buildings. i: Analytical methods. Journal of Geotechnical and Geo-environmental Engineering; 125(1):26–37.

Jacobo B., 1975. Dynamic behavior of structures with embedded foundations. Earthquake Engineering & Structural Dynamics; 3(3):259–274.

Seylabi EE, Jeong C, Taciroglu E., 2016. On numerical computation of impedance functions for rigid soil-structure interfaces embedded in heterogeneous half-spaces. Computers and Geotechnics; 72:15–27.